Offset-Dependent Partial Saturation in Binomial Solvent Suppression Sequences

A. C. Hsu*,†,‡,¶ and C. D. Gregory†,§,¶

*Center for Biophysics and Computational Biology, †Biomedical Magnetic Resonance Laboratory, ‡Medical Scholars Program, §Medical Information Science, and ¶College of Medicine University of Illinois Urbana-Champaign, Urbana, Illinois 61801

In vivo spectroscopic experiments are commonly done under partially T_1 saturated conditions and saturation factors (observed signal intensity divided by fully relaxed intensity) used for quantitative analysis of absolute and relative metabolite concentrations. The conventional calculation of the saturation factor assumes uniform excitation across the spectrum. This assumption is violated when selective-excitation solvent peak suppression techniques, such as binomial sequences, are used. In this case, the degree of partial saturation, and hence the saturation factor, is dependent on the resonance offset. This has implications for the frequency offset of maximum excitation, solvent suppression effectiveness, absolute and relative quantitative measurements, and progressive saturation T_1 measurements. In this paper, the jump and return (JR) and jump and return echo (JRE) sequences are examined in detail with regard to these implications. It is shown that offset-dependent partial saturation depends on the sequence used and can become significant. A saturation factor which is a function of offset can be used to correct for this effect and allow for proper quantitative interpretation of experimental results under partially saturated conditions. © 1998 Academic Press

INTRODUCTION

Over the years, a wide variety methods have been developed for solvent suppression, particularly in ^{1}H spectroscopy of aqueous solutions. Among these are sequences with hard pulse trains, such as jump and return (JR), the family of binomial sequences, and others (*1–7*). Although sequences with shaped pulses, gradients, and phase modulation are popular, the simpler hard pulse sequences are still useful on older instruments with limited pulse-shaping capabilities. The signal amplitude resulting from these sequences (excitation profile) depends on the resonance offset, ω, from the irradiation frequency. For example, JR (*1*) gives a $\sin(\omega\tau)$ profile, $1\bar{3}3\bar{1}$ (*5*) gives a $\sin^3(\omega\tau)$ profile, and $1\bar{1}\,1\bar{1}$ (jump and return echo, JRE) (*6*) gives a $\sin^3(\omega\tau)$ profile. These theoretical profiles are derived by calculating the magnitude of M_{xy} for a single excitation. Since the magnitude of M_{xy} from a single excitation is offset dependent, it is readily apparent that M_z after excitation must be offset dependent

as well. This is of no consequence with sufficiently long repetition times (TR), since M_z would return to its fully relaxed state between excitations. However, short TR values are commonly used in practice. Under these conditions, partial saturation is observed and the nonuniform M_z becomes important.

Quantitative correction for partial saturation can be achieved by dividing the amplitudes or areas of the observed spectral peaks by their respective saturation factors (SF) (*8*), where SF is the partially saturated peak area divided by the fully relaxed peak area. For the simple case of nonselective $\pi/2$ pulses, a saturation factor of

$$\text{SF} = 1 - \exp(-\text{TR}/T_1) \qquad [1]$$

is typically used. However, with the JR and other binomial solvent suppression techniques, the true saturation factor is offset dependent since the steady-state M_z is offset dependent. This paper will examine two pulse sequences, JR and JRE, to investigate the impact of offset-dependent saturation. Although it has been noted that there is an offset-dependent effective flip angle associated with binomial sequences (*9*) and that excitation profiles can be sensitive to T_1 (*10*), to our knowledge a detailed theoretical and experimental examination of these effects and their implications for quantitative analysis and T_1 measurements has not been presented. We will show that in the case of JR, the offset dependence of M_{xy} in the steady state is significantly influenced by partial saturation for short TR values. For JRE, offset-dependent steady state M_{xy} is influenced by partial saturation as well, but to a lesser extent due to EXORCYCLE (*11*) phase cycling. Nevertheless, quantitatively accurate corrections for partial saturation are possible by making the appropriate saturation factor corrections.

THEORY AND METHODS

To evaluate the effects of partial saturation, M_z and M_{xy} were numerically evaluated as a function of offset for the
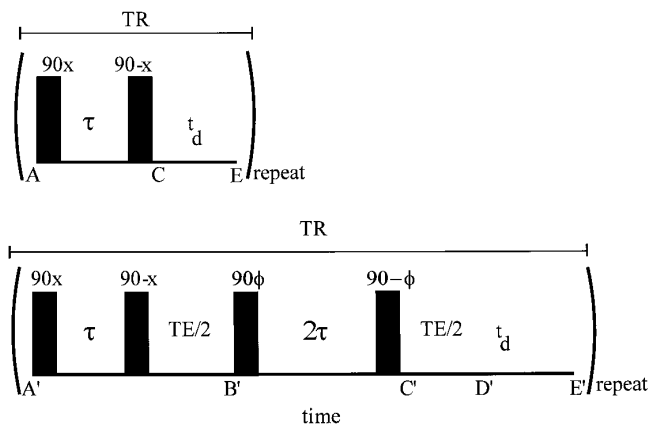
FIG. 1. Pulse sequence timing diagrams for JR and JRE.

JR sequence and for the JRE sequence using a classical vector description. Figure 1 shows the timing diagrams for the two sequences. Since T_1 and T_2 are long compared to the duration of the excitation, relaxation during this portion of the pulse sequence (Fig. 1, A–C and A′–D′) is ignored. The effects of T_1 and T_2 relaxation during selective excitation have been considered by others (12). The RF pulses were assumed to be exactly 90°, of infinitely short duration, and about the proper axis. These assumptions allow for the use of rotation matrices to calculate M_z and M_{xy} in response to excitation (5). Let $\mathbf{R}_\phi(\beta)$ be the matrix for a rotation about the ϕ axis at an angle β in the clockwise direction. For example, $\mathbf{R}_z(\omega\tau)$ represents the effect of precession about the z axis at an offset-dependent rate ω during a delay of

relaxation by T_2 during TR (Fig. 1) occurs, so the magnetization vector is $[0\ 0\ M_{z,n}(0-)]$ immediately prior to the nth excitation. Multiplying this by Eq. [2] gives the magnetization after the nth excitation

$$M_{x,n}(0+) = M_{z,n}(0-)\sin(\omega\tau) \qquad [3]$$

$$M_{y,n}(0+) = 0 \qquad [4]$$

$$M_{z,n}(0+) = M_{z,n}(0-)\cos(\omega\tau) \qquad [5]$$

$$M_{xy,n}(0+) = \sqrt{M_{x,n}^2 + M_{y,n}^2}. \qquad [6]$$

If T_1 relaxation during TR is complete, $M_{z,n}(0-) = M_0$ and the expected excitation profile (1) $S(\omega) = M_0\sin(\omega\tau)$ is obtained from Eq. [6]. T_1 effects are included by setting

$$M_{z,n+1}(0-) = M_{z,n}(0+)$$
$$+ (M_0 - M_{z,n}(0+))(1 - \exp(-\mathrm{TR}/T_1)), \qquad [7]$$

where M_0 is the equilibrium z magnetization. This results in partial saturation, $M_{z,n+1}(0-) < M_0$, being a function of offset, since $M_{z,n}(0+)$ (Eq. [5]) is offset dependent.

JRE Sequence

For JRE, the rotation matrix is $\mathbf{R}_z(\omega\mathrm{TE}/2)\mathbf{R}_{-\phi}(\pi/2)$ $\mathbf{R}_z(\omega2\tau)\mathbf{R}_\phi(\pi/2)\mathbf{R}_z(\omega\mathrm{TE}/2)\mathbf{R}_{-x}(\pi/2)\mathbf{R}_z(\omega\tau)\mathbf{R}_x(\pi/2)$ (Fig. 1, A′–D′). We consider the two pulse groups ($1-\tau-\bar{1}$ and $1-2\tau-\bar{1}$) separately to incorporate phase cycling (6). For the first $1\bar{1}$ pair and the first TE/2 delay (Fig. 1, A′–B′)

$$\mathbf{R}_z(\omega\mathrm{TE}/2)\mathbf{R}_{-x}(\pi/2)\mathbf{R}_z(\omega\tau)\mathbf{R}_x(\pi/2) = \begin{bmatrix} \cos(\omega\mathrm{TE}/2)\cos(\omega\tau) & \sin(\omega\mathrm{TE}/2) & \cos(\omega\mathrm{TE}/2)\sin(\omega\tau) \\ -\sin(\omega\mathrm{TE}/2)\cos(\omega\tau) & \cos(\omega\mathrm{TE}/2) & -\sin(\omega\mathrm{TE}/2)\sin(\omega\tau) \\ -\sin(\omega\tau) & 0 & \cos(\omega\tau) \end{bmatrix}. \qquad [8]$$

length τ. Let $M_{\phi,n}(0-)$ and $M_{\phi,n}(0+)$ be the magnetization component in the ϕ axis direction immediately before and after the nth excitation.

JR Sequence

Excitation for JR (Fig. 1, A–C) is obtained by multiplying the rotations for the two RF pulses and for the intervening delay τ in the order the events occur, giving

$$\mathbf{R}_{-x}(\pi/2)\mathbf{R}_z(\omega\tau)\mathbf{R}_x(\pi/2)$$
$$= \begin{bmatrix} \cos(\omega\tau) & 0 & \sin(\omega\tau) \\ 0 & 1 & 0 \\ -\sin(\omega\tau) & 0 & \cos(\omega\tau) \end{bmatrix}. \qquad [2]$$

If T_2 is short compared to the TR values used, complete

Multiplying the above matrix by the vector $[0\ 0\ M_{z,n}(0-)]$, assuming complete T_2 relaxation during TR, gives at the end of the half-echo delay (Fig. 1, B′)

$$M_{z,n}(0-)\begin{pmatrix} \cos(\omega\mathrm{TE}/2)\sin(\omega\tau) \\ -\sin(\omega\mathrm{TE}/2)\sin(\omega\tau) \\ \cos(\omega\tau) \end{pmatrix}. \qquad [9]$$

Considering only the second $1\bar{1}$ pair (Fig. 1, B′–C′) with EXORCYCLE phase cycling gives (6)

$$\mathbf{R}^E(\phi) = \mathbf{R}_{-\phi}(\pi/2)\mathbf{R}_z(2\omega\tau)\mathbf{R}_\phi(\pi/2) \qquad [10]$$

$$\mathbf{R}^E = \mathbf{R}^E(x) - \mathbf{R}^E(y) + \mathbf{R}^E(-x) - \mathbf{R}^E(-y) \qquad [11]$$

$$\mathbf{R}^{E} = 2 \begin{bmatrix} \cos(2\omega\tau) - 1 & 0 & 0 \\ 0 & 1 - \cos(2\omega\tau) & 0 \\ 0 & 0 & 0 \end{bmatrix} . \quad [12]$$

Multiplying the vector in Eq. [9] by the matrix in Eq. [12] and using Eq. [6] gives $M_{xy,n}(0+) = M_{z,n}(0-)\sin^{3}(\omega\tau)$ for the summed EXORCYCLE phase steps. Note that the summed EXORCYCLE gives M_z of zero because of the plus–minus–plus–minus summing used. However, Eq. [11] and Eq. [12] assume that $M_{z,n}(0-)$ is constant, which is not always true. To determine $M_{x,n}(0+)$, $M_{y,n}(0+)$, and $M_{z,n}(0+)$, the vector in Eq. [9] must be multiplied by $\mathbf{R}^{E}(\phi)$ in Eq. [10] for each of the phase steps, giving

$\pi/2$ pulse with a B_1 field strength of 6.8 kHz, the effect of the finite pulse width on signal amplitude is less than 2% for offsets less than 6.8 kHz (8), but phase varies to a greater degree. For offsets ranging from 0 to 7000 Hz, the phase ranges from 0 to 1 rad for a single $\pi/2$ pulse. To minimize the influence of finite pulse widths on phase and amplitude, we chose to place the excitation maximum at 500 Hz and examine an offset range of −1100 to 1100 Hz. Over this range the amplitude variation is negligible and phase varies from 0 to ±0.16 rad (9°) for a single $\pi/2$ pulse. To simulate accurately a larger offset range, the RF pulse rotation matrices could be replaced with composite rotations corresponding to $\mathbf{B}_{\text{eff}}(\omega) = B_1\mathbf{j}' + (B_0 - \omega/\gamma)\mathbf{k}'$, where $\mathbf{j}'$ and $\mathbf{k}'$ denote the y and z axes in the rotating frame of reference.

$$M_{x,n}(0+) = M_{z,n}(0-) \begin{bmatrix} \sin(\omega\tau)\cos(\omega\text{TE}/2)\cos(2\omega\tau) + \cos(\omega\tau)\sin(2\omega\tau) \\ \sin(\omega\tau)\cos(\omega\text{TE}/2) \\ \sin(\omega\tau)\cos(\omega\text{TE}/2)\cos(2\omega\tau) - \cos(\omega\tau)\sin(2\omega\tau) \\ \sin(\omega\tau)\cos(\omega\text{TE}/2) \end{bmatrix} \quad \text{for } \phi = \begin{matrix} x \\ y \\ -x \\ -y \end{matrix} \quad [13]$$

$$M_{y,n}(0+) = M_{z,n}(0-) \begin{bmatrix} -\sin(\omega\tau)\sin(\omega\text{TE}/2) \\ -\sin(\omega\tau)\sin(\omega\text{TE}/2)\cos(2\omega\tau) + \cos(\omega\tau)\sin(2\omega\tau) \\ -\sin(\omega\tau)\sin(\omega\text{TE}/2) \\ -\sin(\omega\tau)\sin(\omega\text{TE}/2)\cos(2\omega\tau) - \cos(\omega\tau)\sin(2\omega\tau) \end{bmatrix} \quad \text{for } \phi = \begin{matrix} x \\ y \\ -x \\ -y \end{matrix} \quad [14]$$

$$M_{z,n}(0+) = M_{z,n}(0-) \begin{bmatrix} \cos(\omega\tau)\cos(2\omega\tau) - \sin(\omega\tau)\cos(\omega\text{TE}/2)\sin(2\omega\tau) \\ \cos(\omega\tau)\cos(2\omega\tau) + \sin(\omega\tau)\sin(\omega\text{TE}/2)\sin(2\omega\tau) \\ \cos(\omega\tau)\cos(2\omega\tau) + \sin(\omega\tau)\cos(\omega\text{TE}/2)\sin(2\omega\tau) \\ \cos(\omega\tau)\cos(2\omega\tau) - \sin(\omega\tau)\sin(\omega\text{TE}/2)\sin(2\omega\tau) \end{bmatrix} \quad \text{for } \phi = \begin{matrix} x \\ y \\ -x \\ -y \end{matrix} . \quad [15]$$

During TR, T_1 relaxation occurs according to Eq. [7]. Iterations of Eqs. [3]–[7] for JR and Eq. [13]–[15], [6], and [7] for JRE were done with a spreadsheet at values of ω ranging from −1100 to +1100 Hz to obtain the time course of M_{xy} and M_z for each pulse sequence. $\tau = 500 \mu s$, TE = 3.964 ms, and TR/T_1 = 0.5, 1, or 10 were used, to correspond to the experimental conditions below.

Experimental

Experimental measurements were made on a GN-300 wide-bore spectrometer (GE-NMR, Fremont, CA) with a Libra controller (Tecmag, Houston, TX) and a 12-mm broadband probe. $MnCl_2$ (0.15 mL of 0.05 mM) in deionized H_2O in a 5-mm tube was used. Ultem susceptibility plugs (Doty Scientific Inc.) were placed in the NMR tube above and below the sample to limit the sample to the homogeneous B_0 and B_1 region of the decoupler coil. Using inversion recovery and Carr–Purcell–Meiboom–Gill sequences, ^1H T_1 (2.1 s) and T_2 (200 ms) of H_2O were measured.

The $\pi/2$ pulse was carefully determined to be 37 μs (B_1 = 6.8 kHz). For finite pulse widths, offset-dependent phase and amplitude variations were introduced (13). For a single

To generate a signal maximum at an offset of 500 Hz, the interpulse delay τ (Fig. 1) should theoretically be 500 μs for both JR and JRE. However, in addition to phase and amplitude changes, finite pulse widths affect the values used for τ and 2τ. A τ of (500 μs − pulse width) and a 2τ of (1000 μs − pulse width) were used. For the JRE, a TE/2 of 1.982 ms was used. To obtain the excitation profile, the transmitter frequency was set to values ranging from −1100 to +1100 Hz from the water peak frequency, in increments of 100 Hz. For JR, CYCLOPS (14) phase cycling was used, giving 4 scans at each frequency. For JRE, CYCLOPS and EXORCYCLE phase cycling were used giving 16 scans at each frequency. To allow the spins to reach steady state in the short TR experiments, 16 dummy scans were discarded before beginning the signal acquisition at each frequency. TR values of 1.05, 2.1, and 21 s were used to give TR/T_1 ratios of 0.5, 1, and 10. Spectra were calculated by Fourier transform with a line broadening of 10 Hz. Peak areas were determined by Lorentzian fitting using the spectrometer software.

RESULTS

The measured T_1 and T_2 were 2.1 and 0.20 s respectively. This means the assumptions used in the numerical calcula-
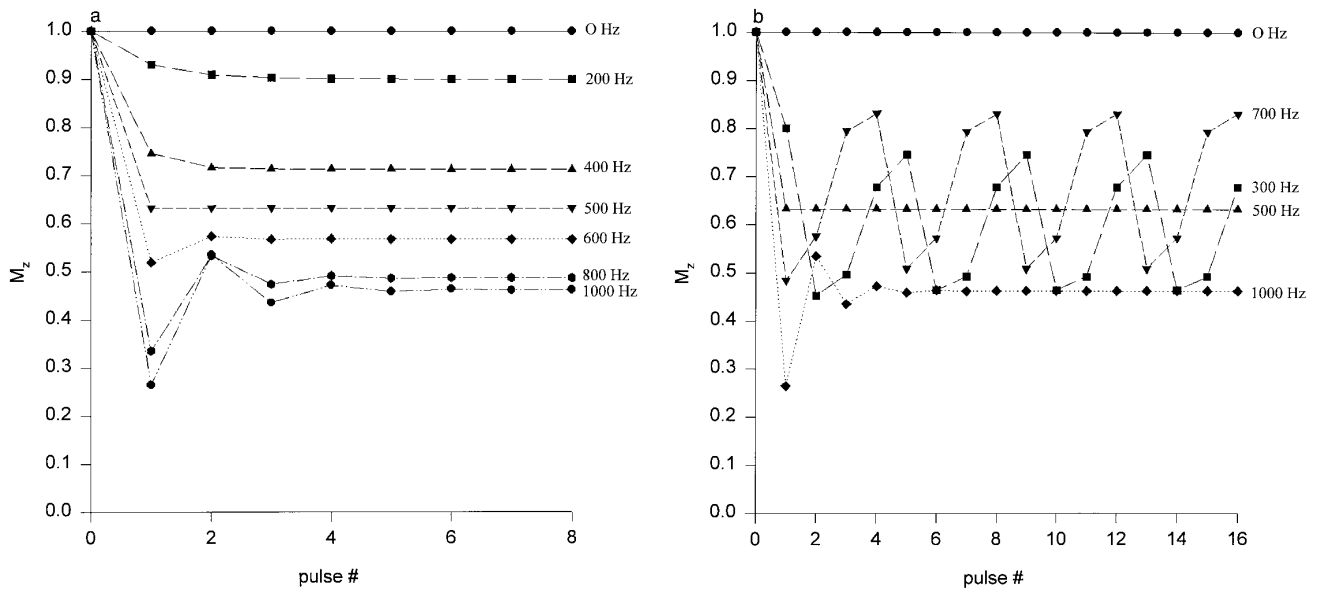
FIG. 2. (a) Calculated time course of $M_{z,n}(0-)$ at different offset frequencies for the JR sequence under partially saturated conditions. $\tau = 500$ μs and TR/$T_1 = 1$. (b) Calculated time course of $M_z(0-)$ at different offset frequencies for the JRE sequence under partially saturated conditions. $\tau = 500$ μs, $2\tau = 1000$ μs, TE/2 = 1.982 ms, and TR/$T_1 = 1$.

tions—no relaxation during excitation, and complete T_2 relaxation during TR—are valid since T_1 and T_2 are long relative to excitation duration and T_2 is short relative to TR for the sequences and conditions we have examined.

The time course of numerically calculated longitudinal magnetization (M_z) in the JR sequence is shown in Fig. 2a as a function of offset frequency for TR/$T_1 = 1$. The frequency-dependent steady state is evident after only a few excitations.

The corresponding numerically calculated frequency-dependent steady state signal (M_{xy}) after excitation is shown as the solid and dashed lines in Fig. 3a, for three different TR/T_1 values. Figure 4a shows the numerically calculated excitation profiles from Fig. 3a with the signal maximum normalized to one at each TR/T_1 value. The overall excitation profile depends on both the excitation offset function $\sin(\omega\tau)$ and the M_z offset function. As seen in Figs. 3a and 4a, a large TR/T_1 gives the expected $\sin(\omega\tau)$ profile since $M_z(0-) = M_0$. However, when TR/T_1 is short, the excitation profile is no longer a simple sine function since $M_z(0-)$ is offset dependent.

Experimentally measured signals as a function of offset are also shown as discrete points in Fig. 3a. For a long TR (TR/$T_1 = 10$), the experimental profile fits a sine function very closely. For short TR values (TR/$T_1 = 0.5$ or 1), the experimentally determined effect of partial saturation can be seen to be in agreement with the theoretical predictions. The signal maximum is shifted significantly toward the center null as TR/T_1 decreases.

The situation differs for JRE. Equation [15] describes M_z reached upon completion of excitation. In addition to the offset dependence, the steady state M_z of the JRE sequence

depends on TE and the order of phase cycling. Figure 2b shows that M_z oscillates with the phase cycle at most offset frequencies. On resonance, M_z does not oscillate and has a magnitude of M_0. At $\omega\tau = \pm\pi/2$ (500 Hz), M_z is also constant upon reaching steady state and behaves as if a Hahn spin echo had been applied. At $\omega\tau = \pm\pi$ (1000 Hz), M_z effectively ''sees'' only the first $1\bar{1}$ pair and hence behaves the same as $\pm\pi$ for JR. The four EXORCYCLE steps largely cancel out the offset-dependent effect on M_z. As a result, upon completion of one EXORCYCLE, the summed M_{xy} is only slightly affected by the frequency dependence of steady state M_z.

Figure 3b compares the simulated M_{xy} of JRE for TR/T_1 = 0.5, 1, and 10 (solid and dashed lines). Figure 4b shows the numerically calculated excitation profiles from Fig. 3b with the signal maximum normalized to one at each TR/T_1 value. TR/$T_1 = 10$ yields the expected $\sin^3(\omega\tau)$ function. For short TR/T_1, the signal maximum is shifted slightly away from the center null as seen in Fig. 4b. The profile is also dependent on TE, but adjusting values of ωTE such that $\sin(\omega$TE$/2)$ and $\cos(\omega$TE$/2)$ range from -1 to 1 only resulted in changes of less than 5% in the excitation profile at offsets ranging from 0 ($\omega\tau = 0$) to 1000 Hz ($\omega\tau = \pi$) at increments of 100 Hz (not shown). Also, since $M_z(0+)$ is dependent on $M_z(0-)$, the order of the phase cycling will alter the excitation profile; again, this effect was small (not shown). Experiments (discrete points in Fig. 3b) showed good agreement with the theoretical predictions of the partial saturation effect.

It should be possible to correct the observed excitation profile by applying a frequency-dependent SF. Such an SF
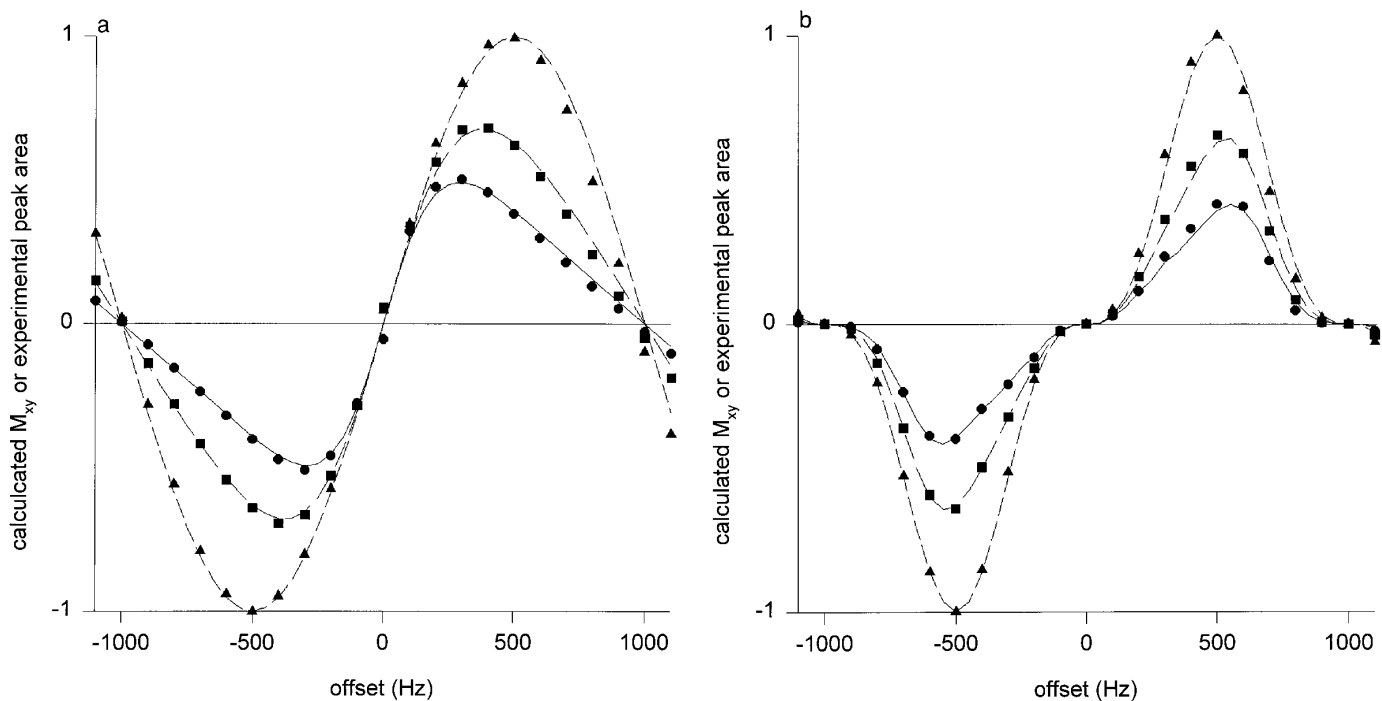
FIG. 3. (a) Calculated offset dependence of steady state M_{xy} for the JR sequence with $\tau = 500$ μs, and TR/$T_1 = 0.5$ (solid line), 1 (long dashes), or 10 (short dashes). Experimental offset dependence of steady state M_{xy} with $\tau = (500$ μs − pulse width), TR/$T_1 = 0.5$ (●), 1 (■), or 10 (▲). (b) Calculated offset dependence of steady state M_{xy} for the JRE sequence with $\tau = 500$ μs, $2\tau = 1000$ μs, TE/2 = 1.982 ms, and TR/$T_1 = 0.5$ (solid line), 1 (long dashes), or 10 (short dashes). Experimental offset dependence of steady state M_{xy} with $\tau = (500$ μs − pulse width), $2\tau = (1000$ μs − pulse width), TE/2 = 1.982 ms, and TR/$T_1 = 0.5$ (●), 1 (■), or 10 (▲).
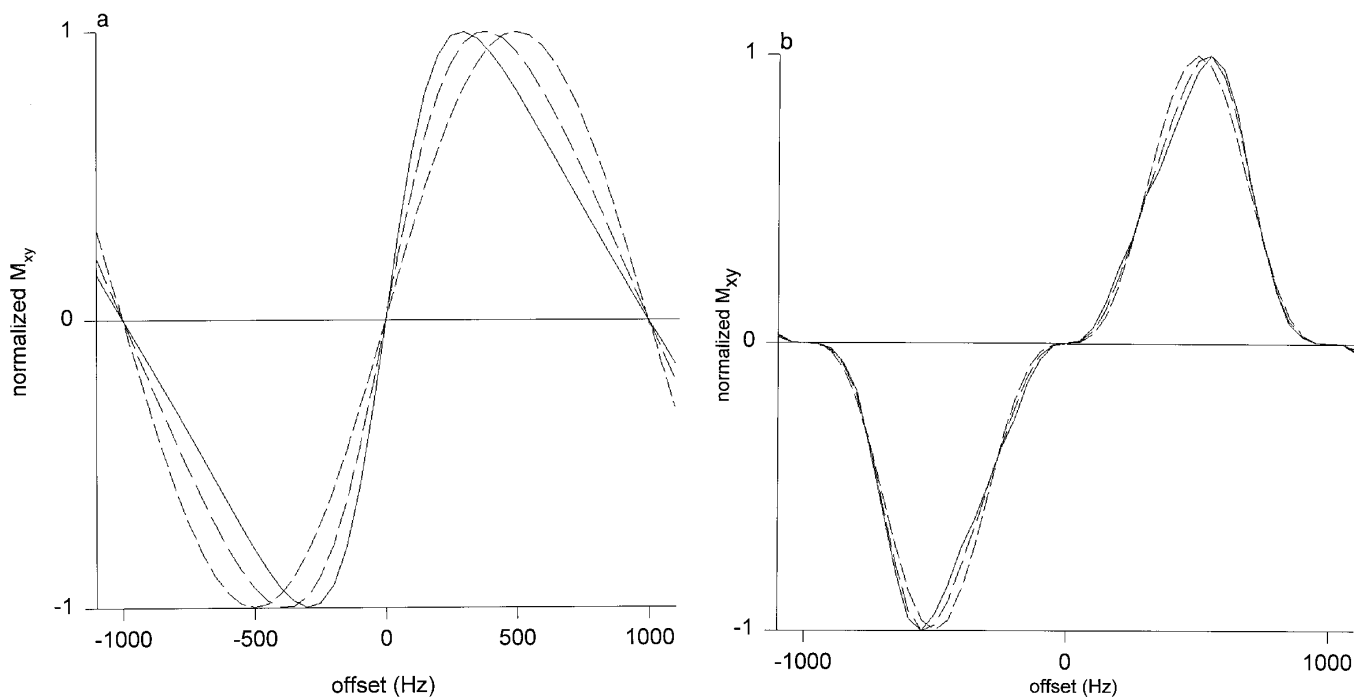
FIG. 4. (a) Calculated offset dependence of steady state M_{xy} for the JR sequence with the maximum M_{xy} normalized to one for TR/$T_1 = 0.5$ (solid lines), 1 (long dashes), and 10 (short dashes). (b) Calculated offset dependence of steady state M_{xy} for the JRE sequence with the maximum M_{xy} normalized to one for TR/$T_1 = 0.5$ (solid lines), 1 (long dashes), and 10 (short dashes).
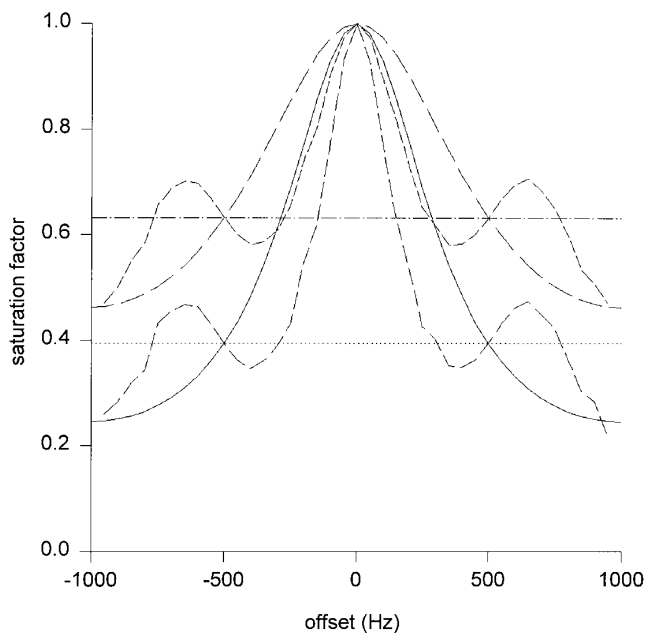
FIG. 5. Calculated SF for JR using $TR/T_1 = 0.5$ (solid line) or 1 (long dashes), $\tau = 500$ μs. Calculated SF for JRE using $TR/T_1 = 0.5$ (medium dashes) or 1 (short dashes), $\tau = 500$ μs, $2\tau = 1000$ μs, $TE/2 = 1.982$ ms. Calculated SF for single $\pi/2$ pulses using $TR/T_1 = 0.5$ (dotted line) or 1 (dash-dot).

may be obtained experimentally, or numerically calculated (Fig. 5). Figure 6a demonstrates that such a correction applied to a JR experiment ($TR/T_1 = 1$) indeed gives good

agreement with the fully relaxed profile. Figure 6b shows similar agreement for the JRE sequence.

DISCUSSION

While T_1 relaxation does not substantially alter the overall excitation profile of the JRE sequence, it does have a significant impact on the profile of JR. This has several implications for use of these sequences for quantitative measurements or for T_1 measurements by progressive saturation.

First, partial saturation affects the frequency at which maximum excitation occurs. Typically, delays (τ) are selected in order to place the peak of greatest interest in a spectrum at the maximum of the excitation profile. However, since T_1 relaxation alters the position of the maximum depending on the TR used, ignoring partial saturation results in a failure to maximize the desired peak. As demonstrated in Figs. 3a and 4a, JR no longer gives a sine profile when TR is short. While the nulls remain at $\omega\tau = 0$, $+\pi$ (1000 Hz), and $-\pi$ (-1000 Hz), the frequency of the maximum response is ''moved'' closer to 0. Since the nulls remain at the same frequency while the frequency of maximum signal is shifted, the profile is no longer symmetrical about the maximum. In contrast, Fig. 4b shows that the overall shape of the excitation profile for JRE still resembles $\sin^3(\omega\tau)$ fairly closely, even under partially saturated conditions. For JRE, the maximum is shifted away from the center null as TR is decreased, but the effect is much less pronounced.

Second, partial saturation affects solvent suppression. Im-
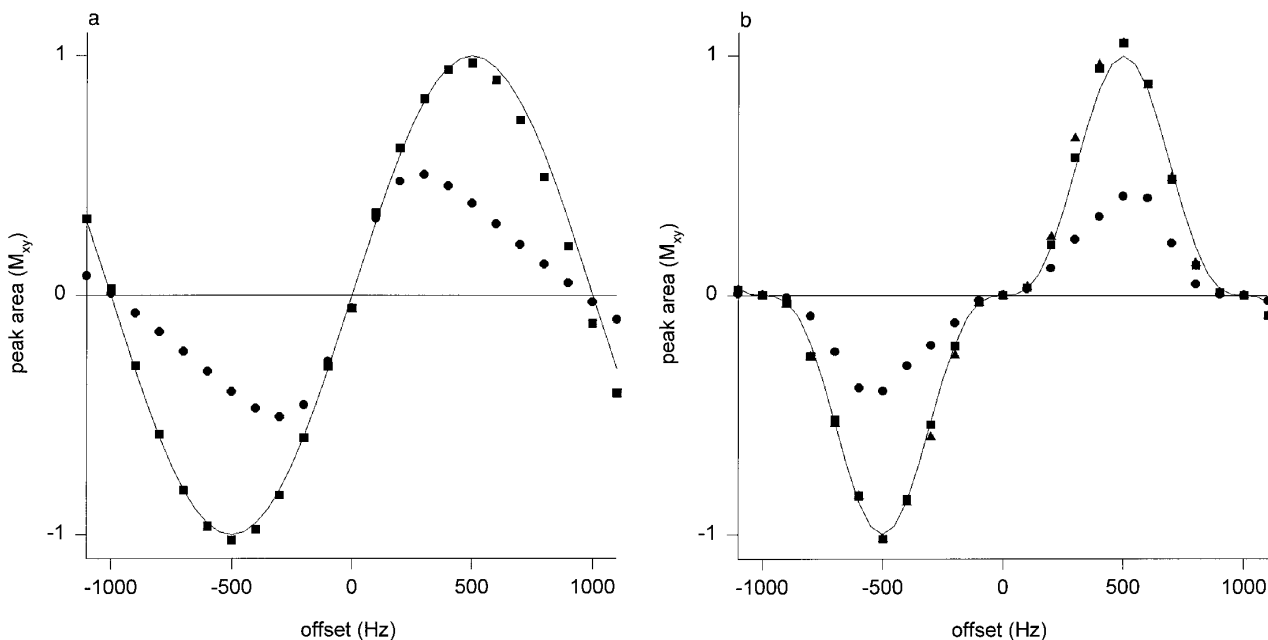
FIG. 6. (a) Experimental response (M_{xy}) from a JR experiment with $TR/T_1 = 0.5$ ($\bullet$). Experiment corrected with SF from Fig. 4 ($\blacksquare$). $\sin(\omega\tau)$ (solid line). (b) Experimental response (M_{xy}) from a JRE experiment for $TR/T_1 = 0.5$ ($\bullet$). Experiment corrected with exact SF from Fig. 4 ($\blacksquare$). Experiment with approximate SF correction ($\blacktriangle$). $\sin^3(\omega\tau)$ (solid line).

mediately following excitation for JR, $M_z(\omega\tau = \pm\pi/2) = 0$ and $M_z(\omega\tau = 0) = 1$. Between $\omega\tau = \pm\pi/2$ and $\omega\tau = 0$ M_z ranges in magnitude from 0 to 1, resulting in a steady state value of $M_{xy}(\omega)$ which is larger than $\sin(\omega\tau)$. The quality of solvent suppression will be adversely affected by this effect if the solvent is placed on resonance, since at frequencies near $\omega\tau = 0$, the signal from the solvent peak tails will be increased relative to the signal maximum (Fig. 4a). For $\pi/2 < \omega\tau < \pi$ and $-\pi/2 > \omega\tau > -\pi$, M_z is negative, ranging from 0 ($\pm\pi/2$) to -1 ($\pm\pi$). The result is a steady state value of $M_{xy}(\omega)$ smaller than $\sin(\omega\tau)$. This suggests that for JR experiments with a short repetition time, solvent suppression could be improved by placing the solvent resonance at $\omega\tau = \pm\pi$ rather than at 0, since the partial saturation effect gives a broader null at $\pm\pi$ than at 0 rad (Fig. 4a). For JRE, signal from frequencies near the center null will also be increased relative to the signal maximum as TR is shortened (Fig. 4b), but to a much lesser degree than for JR.

Third, partial saturation affects quantitative analysis. When attempting to make quantitative measurements, partial saturation correction is made by dividing the observed signal intensities by the saturation factor. For an effective flip angle of α, the saturation factor is

$$\mathrm{SF} = \frac{1 - \exp(-TR/T_1)}{1 - \cos(\alpha)\exp(-TR/T_1)} \qquad [16]$$

where $\cos(\alpha) = (M_z(0+)/M_z(0-))$ (15). For JR and binomial sequences, α becomes a function of offset. In JR, since $M_z(0+) = M_z(0-)\cos(\omega\tau)$ after excitation, α is directly proportional to ω ($\alpha = \omega\tau$), allowing a theoretical $\mathrm{SF}(\omega)$ to be easily calculated (Fig. 5). For JRE the situation is more complex, since α will depend on ω, τ, TE, and EXOR-CYCLE phase steps as seen in Fig. 2b and Eq. [15]. With EXORCYCLE summing of M_x and M_y for the four phase steps, a steady state M_{xy}, which is not substantially affected by TE or phase cycling order, is reached at each frequency. This can be used to calculate the exact numerical $\mathrm{SF}(\omega)$ by using the definition of SF (dividing the calculated short TR steady state EXORCYCLE $M_{xy}(\omega)$ by $\sin^3(\omega\tau)$). Alternatively, the average effective flip angle of the four EXOR-CYCLE phase steps can be derived from Eq. [15] to be $\cos\alpha_{\mathrm{avg}} = \cos(\omega\tau)\cos(2\omega\tau)$, giving a good approximation for SF with Eq. [16]. This is demonstrated in Fig. 6b, which shows correction of experimental data using both ways of calculating SF. Also, SF can be obtained experimentally by comparing short- and long-TR spectral peak amplitudes or areas at a given frequency.

A comparison of the SF for JR, JRE, and $\pi/2$ pulses (Fig. 5) clearly demonstrates the effects of offset-dependent partial saturation. $\mathrm{SF}_{\pi/2} = 0.63$ and 0.39 for $TR/T_1 = 1$ and 0.5 respectively. The maximum difference between $\mathrm{SF}_{\mathrm{JRE}}$ and $\mathrm{SF}_{\pi/2}$ is 12% over the range 210–830 Hz for $TR/T_1 = 1$ and is 21% over the range 220–825 Hz for $TR/T_1 = 0.5$. Regions of deviation from $\mathrm{SF}_{\pi/2}$ over 10% exist as SF for JRE oscillates about 0.63 or 0.39; however, overall $\mathrm{SF}_{\pi/2}$ can be a reasonable approximation for JRE around the signal maximum over a large range. Over the same ranges, JR varies considerably more; $\mathrm{SF}_{\mathrm{JR}}$ varies from 0.48 to 0.89 (-24 to $+41\%$ deviation from 0.63) for $TR/T_1 = 1$ at 210–830 Hz, and from 0.26 to 0.74 (-33 to $+90\%$ deviation from 0.39) for $TR/T_1 = 0.5$ at 220–825 Hz. $\mathrm{SF}_{\pi/2}$ is a good approximation for JR only very near $\omega = \pi/2$ (500 Hz).

Fourth, partial saturation complicates progressive saturation measurements. Progressive saturation determines T_1 by measuring the steady state signal intensity of the desired peak as TR is varied, and by fitting the measurements to an exponential model. In this case, the exponential equation used will depend on the frequency of the peak of interest. The exponential

$$\frac{f(\omega)[1 - \exp(-TR/T_1)]}{1 - \cos(\alpha)\exp(-TR/T_1)} \qquad [17]$$

should be used where $f(\omega)$ is the excitation profile and the effective flip angle α is offset dependent. As already mentioned, $\cos\alpha = \cos(\omega\tau)$ and $\cos\alpha_{\mathrm{avg}} = \cos(\omega\tau)\cos(2\omega\tau)$ for JR and JRE respectively.

CONCLUSION

Offset-dependent partial saturation effects are not negligible in certain binomial water suppression sequences. This has implications for the frequency of maximum excitation, quality of solvent suppression, quantitative analysis, and progressive saturation T_1 measurements. The extent and nature of off-resonance effects depend on details of the pulse sequence. JR, JRE, and other binomial sequences are not isolated examples of offset-dependent partial saturation. Any sequence in which steady state M_z is a function of offset, e.g., sinusoidal-shaped frequency-selective pulses (9) and symmetrically shifted pulses (16), will suffer similar consequences. However, quantitatively accurate corrections for these effects can be made by straightforward numerical methods. The application of such corrections should significantly extend the utility of this class of easily implemented sequences.

REFERENCES

1. P. Plateau and M. Gueron, *J. Am. Chem. Soc.* **104,** 7310 (1982).

2. V. Sklenář and Z. Starcuk, *J. Magn. Reson.* **50,** 495 (1982).

3. G. M. Clore, B. J. Kimber, and A. M. Gronenborn, *J. Magn. Reson.* **54,** 170 (1983).

4. D. Turner, *J. Magn. Reson.* **54,** 146 (1983).

5. P. J. Hore, *J. Magn. Reson.* **55,** 283 (1983).

6. V. Sklenář and A. Bax, *J. Magn. Reson.* **74,** 469 (1987).

7. M. H. Levitt and M. F. Roberts, *J. Magn. Reson.* **71,** 576 (1987).

8. D. G. Gadian, ''NMR and its Applications to Living Systems,'' 2nd ed., p. 218, Oxford Univ. Press, New York (1995).

9. J. Hua and F. J. Ives, *Magn. Reson. Imaging* **14,** 533 (1996).

10. J. H. Gutow, M. McCoy, F. Spano, and W. S. Warren, *Phys. Rev. Lett.* **55,** 1090 (1985).

11. G. Bodenhausen, R. Freeman, and D. L. Turner, *J. Magn. Reson.* **27,** 511 (1977).

12. P. J. Hajduk, D. A. Horita, and L. E. Lerner, *J. Magn. Reson. A* **103,** 40 (1993).

13. E. Fukushima and S. B. W. Roeder, ''Experimental Pulse NMR: A Nuts and Bolts Approach,'' Chap. 2. Addison-Wesley, Reading, MA (1981).

14. D. I. Hoult and D. E. Richards, *Proc. R. Soc. London A* **344,** 311 (1975).

15. R. R. Ernst, G. Bodenhausen, and A. Wokaun, ''Principles of Nuclear Magnetic Resonance in One and Two Dimensions,'' p. 124, Oxford Univ. Press, New York (1994).

16. S. H. Smallcombe, *J. Am. Chem. Soc.* **115,** 4776 (1993).